

GNSS-based Attitude Estimation using Single Baseline

André Oliveira
aoliveira@tecnico.ulisboa.pt

Instituto Superior Técnico, Universidade de Lisboa, Portugal

January 2021

Abstract

The problem of attitude estimation using Global Navigation Satellite Systems (GNSS) has been tackled over the last decades and still draws attention from the navigation community. This work presents the design and preliminary validation of a GNSS-based attitude estimation algorithm suitable for navigation applications, where the performance of said algorithm using a single baseline is highlighted. The proposed solution combines an Extended Kalman Filter (EKF) fed by gyroscope measurements with a state of the art ambiguity determination method. This work's contributions also include an observability analysis of the linearized system's model, where the single baseline case is highlighted. The results obtained for experimental validation of the algorithm are presented, including key conclusions regarding the integer ambiguity determination success, attitude estimation accuracy and further insights on the single baseline observability.

Keywords: Attitude estimation, GNSS, Ambiguity resolution, Filtering, Sensor fusion

1. Introduction

The pros and cons of using GNSS observations for attitude estimation are well known. While the accuracy of a GNSS-based attitude system by itself may not be comparable to other modern solutions, this system is driftless, very low maintenance and considerably less expensive. Global coverage is always available and the reliability of the satellites is guaranteed by ground stations.

Most solutions focus on using at least three GNSS antennas in order to estimate the complete orientation of the body. Using only two antennas, it is generally not possible to do so, unless other sensors such as gyroscopes, accelerometers and magnetometers are used.

In a general way, the GNSS-based attitude estimation methods can be divided into two categories: baseline estimation methods, where the attitude is computed from estimates of the baseline coordinates in the inertial frame, or attitude model-based methods, in which the body attitude is estimated directly from the GNSS observations.

Concerning the first group, a widely used epoch-by-epoch method is detailed in [8], where the baseline coordinates are obtained from a linear least-squares (LS) adjustment. On the other hand, in [7] an Extended Kalman Filter (EKF) is designed in order to estimate the baselines using the GNSS measurements collected over time, such that the baselines are estimated recursively. After obtaining the baseline coordinates in the reference frame, methods such as Davenport's q-method or singular value decomposition-based methods can be used to estimate the rotation that best fits the baselines

[6, 1].

As for the second category, the GNSS-based attitude model is typically the starting point [9]. Variants of this model using a quaternion parametrization of the attitude are also used, in which the estimates are obtained using an iterative LS adjustment or an EKF incorporating a kinematic model [1]. Furthermore, the LS approach introduced by Teunissen in [9] is highlighted, since the present work is based on the same decomposition of the residual squared norm proposed here.

All the enumerated solutions require that the integer ambiguities in the observations model be correctly determined. The methods in the literature usually involve a search algorithm, with some exceptions such as the rounding of the float ambiguities proposed in [1]. Efficient and highly successful integer ambiguity determination (IAD) algorithms were proposed by Teunissen, including the LAMBDA [8], C-LAMBDA [5] and MC-LAMBDA [3] methods. Compared to the first, the other two algorithms introduce constraints regarding known baseline lengths and configuration in order to increase the success rate.

In the present work, a solution based on the novel Multivariate Constrained LAMBDA (MC-LAMBDA) method [3] is proposed, along with a kinematic model integrating rate-gyro measurements. The motivation behind this solution lies with studying how integration of a kinematic model allows full attitude determination using a single baseline in certain scenarios, as well as how it impacts the accuracy of the solution.

2. Problem Definition

Consider a platform where a 3-axis gyroscope and $n + 1$ antennas are mounted. There are static with respect to the body frame coordinate system. Antenna i is designated as the reference antenna. The origin of the body frame coincides with the phase center of the reference antenna.

Let the rotation matrix \mathbf{R} denote the relative orientation between the body frame and the local-level East-North-Up (ENU) frame centered also at the phase center of the reference frame and tangent to the WGS84 ellipsoid. According to the adopted convention, the transformation of vector coordinates between both frames is written as $\mathbf{r}_l = \mathbf{R}\mathbf{r}_b$, where the subscripts l and b denote the local and body frames, respectively.

Following the Hamilton convention, the same rotation is written using the unit quaternion as $\mathbf{r}_l = \mathbf{q} \circ \mathbf{r}_b \circ \mathbf{q}^*$, where $\mathbf{q} = [q_w, \mathbf{q}_v^\top]^\top$, the symbol \circ denotes the quaternion product and \mathbf{q}^* is the quaternion conjugate $\mathbf{q}^* = [q_w - \mathbf{q}_v^\top]^\top$.

Considering that the body frame rotates with respect to the reference frame with angular velocity $\boldsymbol{\omega}(t) = [p(t) \ q(t) \ r(t)]^\top \in \mathbb{R}^3$, measured in the body frame, the time derivative of the unit quaternion is written as in (1). This relation defines the attitude variation between the two frames.

$$\begin{aligned} \dot{\mathbf{q}}(t) &= \frac{1}{2} \begin{bmatrix} 0 \\ \boldsymbol{\omega}(t) \end{bmatrix} \circ \mathbf{q}(t) = \frac{1}{2} \boldsymbol{\Omega}(\boldsymbol{\omega}(t)) \mathbf{q}(t), \\ \boldsymbol{\Omega}(\boldsymbol{\omega}(t)) &= \begin{bmatrix} 0 & -\boldsymbol{\omega}(t)^\top \\ \boldsymbol{\omega}(t) & -[\boldsymbol{\omega}(t) \times] \end{bmatrix} \end{aligned} \quad (1)$$

The GNSS observables providing a measure of the antenna to satellite distance are the pseudorange, or code measurements, and the carrier phase measurements. These quantities are influenced by clock offsets, atmospheric errors and other effects. Some of these errors are mitigated by performing double differences (DD) between measurements of different receivers and satellites. Considering also the short baseline assumption leads to the typical DD observations model (2).

$$\begin{cases} P_{ij}^{kl} = (\mathbf{u}^k - \mathbf{u}^l) \mathbf{b}_{ij} + E_{P,ij}^{kl} \\ \Phi_{ij}^{kl} = (\mathbf{u}^k - \mathbf{u}^l) \mathbf{b}_{ij} + \lambda n_{ij}^{kl} + E_{\Phi,ij}^{kl} \end{cases} \quad (2)$$

In this equation, P_{ij}^{kl} and Φ_{ij}^{kl} denote the DD code and carrier phase measurements, respectively, for receivers i, j and satellites k, l . To build the DD vector, k is set as the reference satellite. The Line of Sight (LOS) vectors \mathbf{u}^k and \mathbf{u}^l point to the respective satellites, and \mathbf{b}_{ij} defines the baseline vector between the two antennas. Lastly, λ is the signal carrier's wavelength and n_{ij}^{kl} the unknown DD integer ambiguities.

Extending this formulation to the $m + 1$ satellites and $n + 1$ receivers, the multiple baseline model is obtained (3), where the DD observations are compacted in matrix \mathbf{Y} , and \mathbf{N} contains the respective DD ambiguities. The baseline coordinates in the reference frame are written

in $\mathbf{B} = [\mathbf{b}_{i1}, \dots, \mathbf{b}_{in}]$. Matrices \mathbf{S} and \mathbf{U} are defined in (4).

$$\begin{cases} \mathbf{Y} = \mathbf{S}\mathbf{N} + \mathbf{U}\mathbf{B} + \boldsymbol{\Xi} & ; \quad \mathbf{Y} \in \mathbb{R}^{2m \times n} \\ \text{Var}(\text{vec}(\mathbf{Y})) = \mathbf{Q}_{\mathbf{Y}\mathbf{Y}} \end{cases} \quad (3)$$

$$\mathbf{S} = \begin{bmatrix} \mathbf{0}_{mn} \\ \lambda \mathbf{I}_{mn} \end{bmatrix}, \quad \mathbf{U} = \begin{bmatrix} \boldsymbol{\Upsilon} \\ \boldsymbol{\Upsilon} \end{bmatrix}, \quad \boldsymbol{\Upsilon} = \begin{bmatrix} \mathbf{u}^k - \mathbf{u}^1 \\ \vdots \\ \mathbf{u}^k - \mathbf{u}^m \end{bmatrix} \quad (4)$$

The $\text{vec}(\cdot)$ operator stacks the columns of the measurements matrix and allows characterizing its uncertainty. Defining the covariance matrices of the code and carrier phase measurements $\text{Var}([P_i^k, \dots, P_i^{m+1}, P_1^k, \dots, P_1^{m+1}, \dots]^\top) = \mathbf{Q}_P$ and the corresponding \mathbf{Q}_Φ as diagonal matrices, an expression for $\mathbf{Q}_{\mathbf{Y}\mathbf{Y}}$ is found. It is written in (5), where $\mathbf{D} = [\mathbf{1}_{m \times 1}, \mathbf{I}_m]$ and $\mathbf{P}_n = \frac{1}{2}(\mathbf{1}_{n \times n} + \mathbf{I}_n)$. Note that $\mathbf{1}_{m \times 1}$ is a $m \times 1$ matrix of ones and \mathbf{I}_m is the identity matrix of dimension m .

$$\mathbf{Q}_{\mathbf{Y}\mathbf{Y}} = \begin{bmatrix} \mathbf{P}_n \otimes 2\mathbf{D}\mathbf{Q}_P\mathbf{D}^\top & \mathbf{0} \\ \mathbf{0} & \mathbf{P}_n \otimes 2\mathbf{D}\mathbf{Q}_\Phi\mathbf{D}^\top \end{bmatrix} \quad (5)$$

As such, the multiple baseline model is fully defined. The algorithm proposed in this article takes advantage of the GNSS-based attitude model mentioned in the Introduction. As such, the matrix of baseline coordinates is replaced in (3) as $\mathbf{B} = \mathbf{R}\mathbf{F}$, where \mathbf{F} contains the known baseline coordinates in the body frame $\mathbf{F} = [l_{i1}, l_{i2}, \dots, l_{in}]$. Minimizing the residual squared norm of the resulting model, a Constrained Integer Least Squares (C-ILS) problem is obtained (6). The proposed solution for this minimization problem is detailed next.

$$\langle \tilde{\mathbf{N}}, \tilde{\mathbf{R}} \rangle = \arg \min_{\mathbf{N} \in \mathbb{Z}^{m \times n}, \mathbf{R} \in \text{SO}(3)} \|\mathbf{Y} - \mathbf{S}\mathbf{N} - \mathbf{U}\mathbf{R}\mathbf{F}\|_{\mathbf{Q}_{\mathbf{Y}\mathbf{Y}}}^2 \quad (6)$$

3. Constrained Integer Least Squares Decomposition for Attitude Estimation

This section describes the key expressions of the proposed solution of the minimization problem. The algorithm is based on the same orthogonal decomposition of the squared norm proposed by Teunissen [9]. Applying the $\text{vec}(\cdot)$ operator so that the Frobenius norm becomes the simpler Euclidean norm, the decomposition is written as

$$\begin{aligned} & \min_{\mathbf{N} \in \mathbb{Z}^{m \times n}, \mathbf{R} \in \text{SO}(3)} \|\text{vec}(\mathbf{Y} - \mathbf{S}\mathbf{N} - \mathbf{U}\mathbf{R}\mathbf{F})\|_{\mathbf{Q}_{\mathbf{Y}\mathbf{Y}}}^2 = \\ & \min \|\text{vec}(\mathbf{Y} - \mathbf{S}\hat{\mathbf{N}} - \mathbf{U}\hat{\mathbf{R}}\mathbf{F})\|_{\mathbf{Q}_{\mathbf{Y}\mathbf{Y}}}^2 + \\ & \min_{\mathbf{N} \in \mathbb{Z}^{m \times n}} \left(\|\text{vec}(\hat{\mathbf{N}} - \mathbf{N})\|_{\hat{\mathbf{Q}}_{\hat{\mathbf{N}}\hat{\mathbf{N}}}}^2 + \right. \\ & \left. \min_{\mathbf{R} \in \text{SO}(3)} \|\text{vec}(\hat{\mathbf{R}}(\mathbf{N}) - \mathbf{R})\|_{\hat{\mathbf{Q}}_{\hat{\mathbf{R}}(\mathbf{N})\hat{\mathbf{R}}(\mathbf{N})}}^2 \right), \end{aligned} \quad (7)$$

where $\hat{\mathbf{N}}$ and $\hat{\mathbf{R}}$ are the float solutions, defined as the solution of the minimization problem in which the integer and nonlinear constraints are dropped (8).

$$\langle \hat{\mathbf{N}}, \hat{\mathbf{R}} \rangle = \arg \min_{\mathbf{N} \in \mathbb{R}^{m \times n}, \mathbf{R} \in \mathbb{R}^{3 \times 3}} \|\text{vec}(\mathbf{Y} - \mathbf{S}\mathbf{N} - \mathbf{U}\mathbf{R}\mathbf{F})\|_{\mathbf{Q}_{\mathbf{Y}\mathbf{Y}}}^2 \quad (8)$$

The conditional rotation matrix $\hat{\mathbf{R}}(\mathbf{N})$ is the solution of the minimization problem in (9) where the integer ambiguities matrix \mathbf{N} is known. Lastly, matrices $\mathbf{Q}_{\hat{\mathbf{N}}\hat{\mathbf{N}}}$ and $\mathbf{Q}_{\hat{\mathbf{R}}(\mathbf{N})\hat{\mathbf{R}}(\mathbf{N})}$ are the respective covariance matrices of $\hat{\mathbf{N}}$ and $\hat{\mathbf{R}}(\mathbf{N})$.

$$\hat{\mathbf{R}}(\mathbf{N}) = \arg \min_{\mathbf{R} \in \mathbb{R}^{3 \times 3}} \|\text{vec}(\mathbf{Y} - \mathbf{S}\mathbf{N} - \mathbf{U}\mathbf{R}\mathbf{F})\|_{\mathbf{Q}_{\mathbf{Y}\mathbf{Y}}}^2 \quad (9)$$

Having $\hat{\mathbf{N}}$ and $\hat{\mathbf{R}}$, the decomposition in (7) allows writing the solution of (6) as

$$\tilde{\mathbf{N}} = \arg \min_{\mathbf{N} \in \mathbb{Z}^{m \times n}} \left(\|\text{vec}(\tilde{\mathbf{N}} - \mathbf{N})\|_{\mathbf{Q}_{\tilde{\mathbf{N}}\tilde{\mathbf{N}}}}^2 + \|\text{vec}(\hat{\mathbf{R}}(\mathbf{N}) - \check{\mathbf{R}}(\mathbf{N}))\|_{\mathbf{Q}_{\hat{\mathbf{R}}(\mathbf{N})\hat{\mathbf{R}}(\mathbf{N})}}^2 \right), \quad (10)$$

with $\check{\mathbf{R}}(\mathbf{N})$ the solution of

$$\check{\mathbf{R}}(\mathbf{N}) = \arg \min_{\mathbf{R} \in \text{SO}(3)} \|\text{vec}(\hat{\mathbf{R}}(\mathbf{N}) - \mathbf{R})\|_{\mathbf{Q}_{\hat{\mathbf{R}}(\mathbf{N})\hat{\mathbf{R}}(\mathbf{N})}}^2. \quad (11)$$

The proposed approach uses a recursive filter to obtain the float solution and employs the MC-LAMBDA algorithm in order to find the integer ambiguities, solution of the minimization problem (10). These are detailed next.

3.1. Nominal System Model

The solution of the minimization problem in (8) is given by an EKF fed by the GNSS observations and employing a kinematic model of the body attitude.

First, the nominal system model is defined. The attitude is parametrized using the unit quaternion, and since the gyroscope measurements are discrete in nature, the kinematic model (1) must be written in discrete-time. The considered rate-gyro stochastic model is written in (12), where $\boldsymbol{\omega}_{m_{k+1}}$ denotes the 3-axes angular velocity measurements at time t_{k+1} , $\boldsymbol{\omega}_{k+1}$ is the true angular velocity and \mathbf{b}_{k+1} denotes the gyro bias. The variables $\mathbf{w}_{v_{k+1}}$ and $\mathbf{w}_{u_{k+1}}$ correspond to white noise processes.

$$\begin{cases} \boldsymbol{\omega}_{m_{k+1}} = \boldsymbol{\omega}_{k+1} + \mathbf{b}_{k+1} + \mathbf{w}_{v_{k+1}} \\ \mathbf{b}_{k+1} = \mathbf{b}_k + \mathbf{w}_{u_{k+1}} \end{cases} \quad (12)$$

Then, based on the derivation in [10] and replacing the angular velocity for the gyro model expression, the quaternion kinematics in discrete-time are approximated by $\mathbf{q}_{k+1} = \bar{\boldsymbol{\Psi}}_{k+1,k} \mathbf{q}_k$, with $\bar{\boldsymbol{\Psi}}_{k+1,k}$ written as

$$\bar{\boldsymbol{\Psi}}_{k+1,k} = \left(\cos \frac{\|\delta\bar{\boldsymbol{\vartheta}}_{k+1,k}\|}{2} \mathbf{I}_4 + \frac{2}{\|\delta\bar{\boldsymbol{\vartheta}}_{k+1,k}\|} \sin \frac{\|\delta\bar{\boldsymbol{\vartheta}}_{k+1,k}\|}{2} \bar{\boldsymbol{\Theta}}_{k+1,k} \right) \quad (13)$$

with $\delta\bar{\boldsymbol{\vartheta}}_{k+1,k}$ and $\bar{\boldsymbol{\Theta}}_{k+1,k}$ defined in (14).

$$\begin{aligned} \delta\bar{\boldsymbol{\vartheta}}_{k+1,k} &= \frac{\Delta t}{2} [(\boldsymbol{\omega}_{m_k} - \bar{\mathbf{b}}_{k,k-1} - \mathbf{w}_{v_k}) + (\boldsymbol{\omega}_{m_{k+1}} - \bar{\mathbf{b}}_{k+1,k} - \mathbf{w}_{v_{k+1}})], \\ \bar{\boldsymbol{\Theta}}_{k+1,k} &= \frac{1}{2} \begin{bmatrix} 0 & -\delta\bar{\boldsymbol{\vartheta}}_{k+1,k}^\top \\ \delta\bar{\boldsymbol{\vartheta}}_{k+1,k} & -[\delta\bar{\boldsymbol{\vartheta}}_{k+1,k} \times] \end{bmatrix} \end{aligned} \quad (14)$$

Defining the state vector of the nominal model as $\mathbf{x}_k = [\mathbf{q}_k^\top, \mathbf{b}_k^\top, \mathbf{n}_k^\top]^\top$, where \mathbf{n}_k is the vector of double differenced integer ambiguities defined as $\mathbf{n}_k \equiv \text{vec}(\mathbf{N})$, the corresponding discrete-time kinematics according to (13) and (12) are written as

$$\mathbf{x}_{k+1} = \begin{bmatrix} \mathbf{q}_{k+1} \\ \mathbf{b}_{k+1} \\ \mathbf{n}_{k+1} \end{bmatrix} = \begin{bmatrix} \bar{\boldsymbol{\Psi}}_{k+1,k} \mathbf{q}_k \\ \mathbf{b}_k + \mathbf{w}_{u_{k+1}} \\ \mathbf{n}_k \end{bmatrix} = \mathbf{f}(\mathbf{x}_k, \mathbf{w}_{v_{k+1}}, \mathbf{w}_{u_{k+1}}) \quad (15)$$

To relate the GNSS observations with the state vector, the rotation in (6) is written using the quaternion product, leading to (16), where the output vector $\mathbf{z}_k \equiv \text{vec}(\mathbf{Y})$ and the measurement noise $\mathbf{v}_k \equiv \boldsymbol{\Xi}$.

$$\mathbf{z}_k = \mathbf{S}\mathbf{n}_k + \mathbf{g}(\mathbf{q}_k) + \mathbf{v}_k = \mathbf{h}(\mathbf{x}_k) + \mathbf{v}_k, \quad (16)$$

$$\mathbf{g}(\mathbf{q}_k) = \begin{bmatrix} \mathbf{1}_2 \otimes \begin{bmatrix} \boldsymbol{\Upsilon} \mathbf{q}_k \circ l_{i1} \circ \mathbf{q}_k^* \\ \vdots \\ \boldsymbol{\Upsilon} \mathbf{q}_k \circ l_{in} \circ \mathbf{q}_k^* \end{bmatrix} \end{bmatrix}$$

3.2. EKF Float Solution

The usual EKF expressions easily follow from the described system. Regarding the propagation step, the predicted state estimate $\hat{\mathbf{x}}_{k|k-1}$ and estimation error covariance matrix $\mathbf{P}_{k|k-1}$ are computed as

$$\hat{\mathbf{x}}_{k|k-1} = \mathbf{f}(\hat{\mathbf{x}}_{k-1|k-1}) \quad (17)$$

$$\mathbf{P}_{k|k-1} = \mathbf{F}_k \mathbf{P}_{k-1|k-1} \mathbf{F}_k^\top + \mathbf{Q}_k,$$

where the nonlinear function $\mathbf{f}(\hat{\mathbf{x}}_{k-1|k-1})$ is written as in (18). Matrix $\boldsymbol{\Psi}^*(\hat{\mathbf{x}}_{k-1|k-1})$ follows from the kinematics (13) evaluated at the previous *a posteriori* estimate $\hat{\mathbf{x}}_{k-1|k-1}$ and omitting the zero-mean noises.

$$\mathbf{f}(\hat{\mathbf{x}}_{k-1|k-1}) = \begin{bmatrix} \boldsymbol{\Psi}^*(\hat{\mathbf{x}}_{k-1|k-1}) \hat{\mathbf{q}}_{k-1|k-1} \\ \hat{\mathbf{b}}_{k-1|k-1} \\ \hat{\mathbf{n}}_{k-1|k-1} \end{bmatrix} \quad (18)$$

Matrix \mathbf{F}_k results from the Jacobian of the nominal system model with regards to the state vector. The model is only nonlinear with respect to the gyro bias and the respective derivative is given by

$$\begin{aligned} \frac{\partial \bar{\mathbf{f}}(\mathbf{q}_k, \mathbf{b}_k, \mathbf{w}_{v_{k+1}})}{\partial \mathbf{b}_k} &= \mathbf{L}(\mathbf{q}_k, \mathbf{b}_k) = \frac{\Delta t \sin \frac{\|\delta\bar{\boldsymbol{\vartheta}}_{k+1,k}\|}{2}}{2 \|\delta\bar{\boldsymbol{\vartheta}}_{k+1,k}\|} \\ &[\mathbf{q}_k \delta\bar{\boldsymbol{\vartheta}}_{k+1,k}^\top - 2\boldsymbol{\Gamma}(\mathbf{q}_k)] - \frac{\Delta t}{2 \|\delta\bar{\boldsymbol{\vartheta}}_{k+1,k}\|^2} \left[\cos \frac{\|\delta\bar{\boldsymbol{\vartheta}}_{k+1,k}\|}{2} \right. \\ &\left. \frac{2}{\|\delta\bar{\boldsymbol{\vartheta}}_{k+1,k}\|} \sin \frac{\|\delta\bar{\boldsymbol{\vartheta}}_{k+1,k}\|}{2} \right] \boldsymbol{\Gamma}(\mathbf{q}_k) \delta\bar{\boldsymbol{\vartheta}}_{k+1,k} \delta\bar{\boldsymbol{\vartheta}}_{k+1,k}^\top, \end{aligned} \quad (19)$$

which leads to the matrix \mathbf{F}_k defined in (20).

$$\mathbf{F}_k = \left[\begin{array}{ccc} \Psi^*(\mathbf{x}_k) & \mathbf{L}(\mathbf{x}_k) & \mathbf{0} \\ \mathbf{0} & \mathbf{I} & \mathbf{0} \\ \mathbf{0} & \mathbf{0} & \mathbf{I} \end{array} \right] \Big|_{\mathbf{x}_k = \hat{\mathbf{x}}_{k-1|k-1}} \quad (20)$$

Note that $\Delta t = t_{k+1} - t_k$. Assuming a small sampling interval, \mathbf{Q}_k is approximated as $\mathbf{Q}_k = \mathbf{G}_k \mathbf{Q} \mathbf{G}_k^\top \Delta t$, where \mathbf{G}_k is the noise scaling matrix of the continuous-time model (21) and \mathbf{Q} is the covariance matrix of the multivariate random vector of white noise processes $\boldsymbol{\eta}(t) = [\boldsymbol{\eta}_v(t)^\top, \boldsymbol{\eta}_w(t)^\top]^\top$.

$$\dot{\mathbf{x}}(t) = \begin{bmatrix} \frac{1}{2} \boldsymbol{\Omega}(\mathbf{w}_m(t) - \mathbf{b}(t)) & \mathbf{0} & \mathbf{0} \\ \mathbf{0} & \mathbf{0} & \mathbf{0} \\ \mathbf{0} & \mathbf{0} & \mathbf{0} \end{bmatrix} \mathbf{x}(t) + \mathbf{G}(t) \boldsymbol{\eta}(t),$$

$$\mathbf{G}(t) = \begin{bmatrix} -\frac{1}{2} \boldsymbol{\Gamma}(\mathbf{q}(t)) & \mathbf{0} \\ \mathbf{0} & \mathbf{I} \\ \mathbf{0} & \mathbf{0} \end{bmatrix}, \boldsymbol{\Gamma}(\mathbf{q}) = \begin{bmatrix} -q_x & -q_y & -q_z \\ q_w & -q_z & q_y \\ q_z & q_w & -q_x \\ -q_y & q_x & q_w \end{bmatrix} \quad (21)$$

The update step is defined by the expressions in (22), used to compute the *a posteriori* estimates of the state vector $\hat{\mathbf{x}}_{k|k}$ and the estimation error covariance matrix $\mathbf{P}_{k|k}$.

$$\mathbf{K}_k = \mathbf{H}_k^\top (\mathbf{H}_k \mathbf{P}_{k|k-1} \mathbf{H}_k^\top + \mathbf{R}_k)^{-1} \quad (22)$$

$$\hat{\mathbf{x}}_{k|k} = \hat{\mathbf{x}}_{k|k-1} + \mathbf{K}_k (z_k - \mathbf{h}(\hat{\mathbf{x}}_{k|k-1}))$$

$$\mathbf{P}_{k|k} = (\mathbf{I} - \mathbf{K}_k \mathbf{H}_k) \mathbf{P}_{k|k-1}$$

The predicted measurements $\mathbf{h}(\hat{\mathbf{x}}_{k|k-1})$ are computed using the nonlinear output equation (16) evaluated at $\hat{\mathbf{x}}_{k|k-1}$. This model is nonlinear with respect to the quaternion. The derivative of the nonlinear term is written in (23), which along with the output equation (16) leads to the \mathbf{H}_k matrix in (24).

$$\frac{d}{dq} \mathbf{g}(\mathbf{q}) = \left[\mathbf{1}_2 \otimes \begin{bmatrix} \boldsymbol{\Upsilon} \mathbf{J}_q(\mathbf{q}, l_{i1}) \\ \vdots \\ \boldsymbol{\Upsilon} \mathbf{J}_q(\mathbf{q}, l_{in}) \end{bmatrix} \right] = \mathbf{G}'(\mathbf{q}), \quad (23)$$

$$\frac{\mathbf{J}_q(\mathbf{q}, l)}{2} = [q_w l - [l \times] q_v, -q_w [l \times] + q_v^\top \mathbf{I} + q_v l^\top - l q_v^\top]$$

$$\mathbf{H}_k = [\mathbf{G}'(\mathbf{x}_k) \quad \mathbf{0} \quad \mathbf{S}] \Big|_{\mathbf{x}_k = \hat{\mathbf{x}}_{k|k-1}} \quad (24)$$

Lastly, the measurements noise covariance matrix \mathbf{R}_k is equivalent to $\mathbf{Q}_{\mathbf{Y}\mathbf{Y}}$.

3.3. Observability Analysis for Single vs Multiple Baseline

Since the system model is nonlinear, rigorous analysis of its observability properties requires using tools such as the *observability rank condition* [4]. Doing so for this system which is used to estimate both the attitude, gyro bias and integer ambiguities is not trivial. Therefore, a simplified analysis using a linearized model is done.

Let $\tilde{\mathbf{x}}_k = [\tilde{\mathbf{q}}_k^\top, \tilde{\mathbf{b}}_k^\top, \tilde{\mathbf{n}}_k^\top]^\top$ be the state vector corresponding to an operation point of the considered system. Then, the trajectory of the system along this operation point obeys the state vector dynamics written in (15). A deviation from the operation point, $\Delta \mathbf{x}_{k+1} = \mathbf{x}_{k+1} - \tilde{\mathbf{x}}_{k+1}$, can be locally approximated by $\Delta \mathbf{x}_{k+1} \approx \boldsymbol{\Phi} \Delta \mathbf{x}_k$, where $\boldsymbol{\Phi}$ coincides with the Jacobian matrix in (20) evaluated at $\mathbf{x}_k = \tilde{\mathbf{x}}_k$.

Similarly, the perturbation of the measurements can be written as $\Delta \mathbf{z}_k = \mathbf{H} \Delta \mathbf{x}_k$, where \mathbf{H} is the output equation's Jacobian in (24) also evaluated at $\mathbf{x}_k = \tilde{\mathbf{x}}_k$.

A simple criteria for analyzing the observability of an LTI system is given in [2] and consists of computing the rank of the observability matrix \mathcal{O} defined as

$$\mathcal{O} = \begin{bmatrix} \mathbf{H} \\ \mathbf{H} \boldsymbol{\Phi} \\ \vdots \\ \mathbf{H} \boldsymbol{\Phi}^{n-1} \end{bmatrix}, \quad (25)$$

where n is the dimension of the system's state vector. If \mathcal{O} is full rank, that is, $\text{rank } \mathcal{O} = n$, then the linear system is observable. It is known that if the matrix is full rank, then the kernel of \mathcal{O} must have dimension 0. That is, the only solution of the system $\mathcal{O} \mathbf{x}$ must be $\mathbf{x} = \mathbf{0}$. Replacing the expressions for $\boldsymbol{\Phi}$ and \mathbf{H} , derived from (20) and (24), allows writing the system of equations as

$$\begin{bmatrix} \mathbf{G}' & \mathbf{0} & \mathbf{S} \\ \mathbf{G}' \Psi^* & \mathbf{G}' \mathbf{L} & \mathbf{0} \\ \vdots & \vdots & \vdots \\ \mathbf{G}' (\Psi^*)^{n-1} & \mathbf{G}' ((\Psi^*)^{n-2} + \dots + \mathbf{I}) \mathbf{L} & \mathbf{0} \end{bmatrix} \mathbf{x} = \mathbf{0} \quad (26)$$

where $\mathbf{x} = [\mathbf{x}_1^\top, \mathbf{x}_2^\top, \mathbf{x}_3^\top]^\top$ according to the three column blocks. From this point on, the single and multiple baseline cases can be discriminated.

3.3.1 Single Baseline

Considering a single baseline l_{12} , \mathbf{G}' is written as

$$\mathbf{G}' = [\mathbf{1}_2 \otimes [\boldsymbol{\Upsilon} \mathbf{J}_q(\mathbf{q}_k, l_{12})]] \Big|_{\mathbf{x}_k = \tilde{\mathbf{x}}_k}. \quad (27)$$

Replacing the expressions for \mathbf{G}' and \mathbf{S} , the first line of equations from system (26) reads

$$\begin{bmatrix} \boldsymbol{\Upsilon} \mathbf{J}_q(\tilde{\mathbf{q}}_k, l_{12}) \mathbf{x}_1 + \mathbf{0}_m \mathbf{x}_3 \\ \boldsymbol{\Upsilon} \mathbf{J}_q(\tilde{\mathbf{q}}_k, l_{12}) \mathbf{x}_1 + \lambda \mathbf{I}_m \mathbf{x}_3 \end{bmatrix} = \begin{bmatrix} \mathbf{0} \\ \mathbf{0} \end{bmatrix} = \Delta \mathbf{z}_k. \quad (28)$$

Naturally, this system corresponds to finding the points where the observations of the linearized system are equal to $\mathbf{0}$. For convenience, define $\mathbf{x}_1 \equiv \Delta \mathbf{q}_k$ and $\mathbf{x}_3 \equiv \Delta \mathbf{n}_k$. It follows from (28) that $\mathbf{x}_3 = \mathbf{0}$. The goal is then to find the admissible perturbations from the operation point $\Delta \mathbf{q}_k$ that make the measurements variation null. Consider that there is a clear line of sight

to at least four non-planar satellites, so that Υ is full rank. Also note that in a local sense, the LOS vectors vary very slowly and can be considered approximately constant. Taking into account the physical meaning of the observations, it is simple to realize that if the variation in attitude from $\tilde{\mathbf{q}}_k$ to \mathbf{q}_k ($\Delta\mathbf{q}_k$) corresponds to a rotation around an axis collinear to the baseline \mathbf{l}_{12} , the coordinates of the baseline do not change, which implies $\Delta\mathbf{z}_k = \mathbf{0}$. As such, the solution of (28) is written as

$$\begin{cases} \mathbf{x}_1 = \Delta\mathbf{q}_k = \tilde{\mathbf{q}}_k \circ \mathbf{q}\{\alpha\mathbf{l}_{12}\} - \tilde{\mathbf{q}}_k, & \forall \alpha \in \mathbb{R} \\ \mathbf{x}_3 = \Delta\mathbf{n}_k = \mathbf{0} \end{cases} \quad (29)$$

where $\mathbf{q}\{\alpha\mathbf{l}_{12}\}$ denotes a rotation around the axis defined by \mathbf{l}_{12} of magnitude $\alpha\|\mathbf{l}_{12}\|$.

Then, the second line of equations reads

$$\mathbf{G}'\Psi^*\mathbf{x}_1 + \mathbf{G}'\mathbf{L}\mathbf{x}_2 = \mathbf{0}. \quad (30)$$

The product

$$\Psi^*\mathbf{x}_1 = \Psi^*\Delta\mathbf{q}_k = \Psi^*(\tilde{\mathbf{q}}_k \circ \mathbf{q}\{\alpha\mathbf{l}_{12}\} - \tilde{\mathbf{q}}_k) \quad (31)$$

can be recognized as the quaternion kinematics equation applied to both $\tilde{\mathbf{q}}_k \circ \mathbf{q}\{\alpha\mathbf{l}_{12}\}$ and $\tilde{\mathbf{q}}_k$. The attitude given by these quaternions is changed according to the angular velocity of the body used to compute Ψ^* . Considering that the linearization is done around a trajectory where the body is rotating around \mathbf{l}_{12} , or is static, then $\Delta\mathbf{q}' = \Psi^*\Delta\mathbf{q}_k$ still corresponds to a difference in rotation around \mathbf{l}_{12} . In this case, $\mathbf{G}'\Psi^*\mathbf{x}_1 = \mathbf{0}$. The same reasoning applies to successive rotations $\mathbf{G}'(\Psi^*)^k\Delta\mathbf{q}_k$, for $k > 1$, giving the conclusion of non-observability for the attitude. Then, to solve for \mathbf{x}_2 in (30), the particular case where the body is static is analyzed, simplifying the equation $\mathbf{G}'\mathbf{L}\mathbf{x}_2 = \mathbf{0}$ to

$$-\frac{\Delta t}{2}\Upsilon\mathbf{J}_q(\tilde{\mathbf{q}}_k, \mathbf{l}_{12})\mathbf{\Gamma}(\tilde{\mathbf{q}}_k)\mathbf{x}_2 = \mathbf{0}, \quad (32)$$

with $\mathbf{\Gamma}$ defined in (19). Further manipulation of this expression leads to

$$\Upsilon\mathbf{R}(\tilde{\mathbf{q}}_k)[\mathbf{l}_{12} \times] \mathbf{x}_2 = \mathbf{0}, \quad (33)$$

where $\mathbf{R}(\tilde{\mathbf{q}}_k)$ denotes the quaternion parametrization of the rotation matrix. Since Υ is full rank, the only solution to $\Upsilon\mathbf{r} = \mathbf{0}$ is $\mathbf{r} = \mathbf{0}$. Therefore, the trivial solution $\mathbf{x}_2 = c_1\mathbf{l}_{12}$, $\forall c_1 \in \mathbb{R}$ naturally follows.

It is inferred from the linearized model that, in a single baseline scenario, if the body is rotating around the axis defined by the baseline or is static, the attitude is not observable, having one degree of freedom. If, in particular, it is static, the bias is also not observable. A more general conclusion is left for future work.

3.3.2 Multiple Baseline

The following analysis, done for two baselines \mathbf{l}_{12} and \mathbf{l}_{13} , is easily extended for three or more. In this case,

\mathbf{G}' is written as

$$\mathbf{G}' = \left[\mathbf{1}_2 \otimes \begin{bmatrix} \Upsilon\mathbf{J}_q(\mathbf{q}_k, \mathbf{l}_{12}) \\ \Upsilon\mathbf{J}_q(\mathbf{q}_k, \mathbf{l}_{13}) \end{bmatrix} \right] \Big|_{\mathbf{x}_k = \tilde{\mathbf{x}}_k}. \quad (34)$$

Replacing this expression, the first line of system (26) becomes

$$\begin{bmatrix} \Upsilon\mathbf{J}_q(\tilde{\mathbf{q}}_k, \mathbf{l}_{12})\Delta\mathbf{q}_k + \mathbf{0}_m\Delta\mathbf{n}_k \\ \Upsilon\mathbf{J}_q(\tilde{\mathbf{q}}_k, \mathbf{l}_{12})\Delta\mathbf{q}_k + \lambda\mathbf{I}_m\Delta\mathbf{n}_k \\ \Upsilon\mathbf{J}_q(\tilde{\mathbf{q}}_k, \mathbf{l}_{13})\Delta\mathbf{q}_k + \mathbf{0}_m\Delta\mathbf{n}_k \\ \Upsilon\mathbf{J}_q(\tilde{\mathbf{q}}_k, \mathbf{l}_{13})\Delta\mathbf{q}_k + \lambda\mathbf{I}_m\Delta\mathbf{n}_k \end{bmatrix} = \begin{bmatrix} \mathbf{0} \\ \mathbf{0} \\ \mathbf{0} \\ \mathbf{0} \end{bmatrix}, \quad (35)$$

where again it was defined $\mathbf{x}_1 \equiv \Delta\mathbf{q}_k$ and $\mathbf{x}_3 \equiv \Delta\mathbf{n}_k$. The first two lines refer to the variation in observations $\Delta\mathbf{z}_k^{12}$, related to \mathbf{l}_{12} , while the last two refer to $\Delta\mathbf{z}_k^{13}$.

The same rationale as before is applied. If $\Delta\mathbf{q}_k$ corresponds to a rotation around \mathbf{l}_{12} , then $\Delta\mathbf{z}_k^{12} = \mathbf{0}$. However, if \mathbf{l}_{12} and \mathbf{l}_{13} are not collinear, then this $\Delta\mathbf{q}_k$ entails $\Delta\mathbf{z}_k^{13} \neq \mathbf{0}$, since the coordinates of the baseline \mathbf{l}_{13} in the reference frame will change. The inverse applies if $\Delta\mathbf{q}_k$ is defined as a rotation around \mathbf{l}_{13} . Therefore, for non-collinear baselines, the only solution is $\Delta\mathbf{q}_k = \mathbf{x}_1 = \mathbf{0}$.

To solve for \mathbf{x}_2 , the second line of equations in (26) is analysed. Since $\mathbf{x}_1 = \mathbf{0}$, and again studying the static scenario, the same simplifications as in the single baseline case apply. The system to solve becomes

$$\begin{bmatrix} \Upsilon\mathbf{R}(\tilde{\mathbf{q}}_k)[\mathbf{l}_{12} \times] \mathbf{x}_2 = \mathbf{0} \\ \Upsilon\mathbf{R}(\tilde{\mathbf{q}}_k)[\mathbf{l}_{13} \times] \mathbf{x}_2 = \mathbf{0} \end{bmatrix} = \begin{bmatrix} \mathbf{0} \\ \mathbf{0} \end{bmatrix}. \quad (36)$$

Assuming that Υ is full rank, if \mathbf{l}_{12} and \mathbf{l}_{13} are not collinear, the only solution is clearly $\mathbf{x}_2 = \mathbf{0}$.

In the multiple baseline case, it is concluded that, without imposing any restrictions on the trajectory of the linearization, the attitude is observable. If the body is static, it is found that the gyro bias is also observable. Intuitively, this should remain true under any other condition, although the analytical proof is left for future work.

3.4. Integer Ambiguity Determination

Due to the decomposition of the error squared norm in (7), the integer ambiguity determination problem consists of solving the minimization problem defined in (10). The MC-LAMBDA is an efficient search algorithm which solves this problem. In the following, only the decisions made which are particular to this work are described. For the full description of the method, refer to [3].

First, consider the cost function to minimize, written from (10) as

$$C(\mathbf{N}) = \|\text{vec}(\hat{\mathbf{N}} - \mathbf{N})\|_{\mathbf{Q}_{\hat{\mathbf{N}}\hat{\mathbf{N}}}}^2 + \|\text{vec}(\hat{\mathbf{R}}(\mathbf{N}) - \check{\mathbf{R}}(\mathbf{N}))\|_{\mathbf{Q}_{\hat{\mathbf{R}}(\mathbf{N})\hat{\mathbf{R}}(\mathbf{N})}}^2, \quad (37)$$

where $\check{\mathbf{R}}(\mathbf{N})$ the solution of (11). Being a minimization problem with integer constraints, the solution is found

by performing a search on the ambiguities' search space defined in (38).

$$\Omega^C(\chi^2) = \{\mathbf{N} \in \mathbb{Z}^{m \times n} \mid C(\mathbf{N}) \leq \chi^2\} \quad (38)$$

The computational cost of the algorithm is related to the choice of χ^2 , which defines the volume of the search space. For each candidate in $\Omega^C(\chi^2)$, the cost function $C(\mathbf{N})$ must be evaluated, which entails solving the nonlinear minimization problem (11). To improve the efficiency of the search, easier to evaluate bounding functions are proposed, such that $C_1(\mathbf{N}) \leq C(\mathbf{N}) \leq C_2(\mathbf{N})$. In this work, the cost function $C_1(\mathbf{N})$ in (39) is used, where λ_m is the smallest eigenvalue of $\mathbf{Q}_{\hat{\mathbf{R}}(\mathbf{N})\hat{\mathbf{R}}(\mathbf{N})}^{-1}$ and $\hat{\mathbf{r}}_i(\mathbf{N})$ are the column vectors of $\hat{\mathbf{R}}(\mathbf{N})$.

$$C_1(\mathbf{N}) = \|\text{vec}(\hat{\mathbf{N}} - \mathbf{N})\|_{\mathbf{Q}_{\hat{\mathbf{N}}\hat{\mathbf{N}}}}^2 + \lambda_m \sum_{i=1}^3 (\|\hat{\mathbf{r}}_i(\mathbf{N})\| - 1)^2 \quad (39)$$

Based on this bounding cost function, the *Expansion* approach, detailed in [3], is used. Note that the efficiency of the search algorithm depends on the tightness of $C_1(\mathbf{N})$ in relation to $C(\mathbf{N})$. If the eigenvalues of $\mathbf{Q}_{\hat{\mathbf{R}}(\mathbf{N})\hat{\mathbf{R}}(\mathbf{N})}^{-1}$ range across several orders of magnitude, a different bound should be used.

Having enumerated these decisions, some issues remain to be tackled. The expressions for the conditional solution $\hat{\mathbf{R}}(\mathbf{N})$ and its respective covariance matrix $\mathbf{Q}_{\hat{\mathbf{R}}(\mathbf{N})\hat{\mathbf{R}}(\mathbf{N})}$ derived in [3] are obtained assuming that LS adjustment is used to compute the float solution. In this work, the float solution is given by an EKF. Furthermore, to allow using this method in a single baseline scenario, the solution of (9) must be linked to the EKF float solution. Therefore, new expressions for these matrices are derived. This problem is addressed in the following.

3.4.1 Obtaining the conditional solution

To describe how the EKF estimates lead to $\hat{\mathbf{R}}(\mathbf{N})$ and $\mathbf{Q}_{\hat{\mathbf{R}}(\mathbf{N})\hat{\mathbf{R}}(\mathbf{N})}$, consider the float and conditional solution minimization problems formulated using a quaternion parametrization of the attitude, written in (40) and (41), respectively. Note that, for simplicity, $\mathbf{y} \equiv \text{vec}(\mathbf{Y})$ and $\mathbf{n} \equiv \text{vec}(\mathbf{N})$.

$$\langle \hat{\mathbf{n}}, \hat{\mathbf{q}} \rangle = \arg \min_{\mathbf{n} \in \mathbb{R}^{mn}, \mathbf{q} \in \mathbb{R}^4} \|\mathbf{y} - \mathbf{S}\mathbf{n} - \mathbf{g}(\mathbf{q})\|_{\mathbf{Q}_{\mathbf{Y}\mathbf{Y}}}^2 \quad (40)$$

$$\hat{\mathbf{q}}(\mathbf{n}) = \arg \min_{\mathbf{q} \in \mathbb{R}^4} \|\mathbf{y} - \mathbf{S}\mathbf{n} - \mathbf{g}(\mathbf{q})\|_{\mathbf{Q}_{\mathbf{Y}\mathbf{Y}}}^2 \quad (41)$$

Then, both nonlinear models are linearized and the minimization problems are solved using the Gauss-Newton method. Considering that the first guess of the quaternion is the same in both problems, and that it is

a good estimate of the solution, it is possible to write a conditional solution $\mathbf{q}(\mathbf{N})$ and its respective covariance matrix $\mathbf{Q}_{\mathbf{q}(\mathbf{N})\mathbf{q}(\mathbf{N})}$ as a function of the float solution. These expressions are written in (42) and (43).

$$\mathbf{q}(\mathbf{N}) = \hat{\mathbf{q}} - \mathbf{Q}_{\hat{\mathbf{q}}\hat{\mathbf{N}}}\mathbf{Q}_{\hat{\mathbf{N}}\hat{\mathbf{N}}}^{-1} \left(\text{vec}(\hat{\mathbf{N}} - \mathbf{N}) \right) \quad (42)$$

$$\mathbf{Q}_{\mathbf{q}(\mathbf{N})\mathbf{q}(\mathbf{N})} = \mathbf{Q}_{\hat{\mathbf{q}}\hat{\mathbf{q}}} - \mathbf{Q}_{\hat{\mathbf{q}}\hat{\mathbf{N}}}\mathbf{Q}_{\hat{\mathbf{N}}\hat{\mathbf{N}}}^{-1}\mathbf{Q}_{\hat{\mathbf{N}}\hat{\mathbf{q}}} \quad (43)$$

Then, it is assumed that the solution of (40) can be replaced by the designed EKF. As such, the covariance matrices of the float solution in (42) and (43) are extracted from $\mathbf{P}_{k|k}$, and $\hat{\mathbf{q}}$, $\hat{\mathbf{N}}$ are the EKF estimates. Afterwards, $\mathbf{R}(\mathbf{N})$ and the respective covariance matrix are computed from $\mathbf{q}(\mathbf{N})$ and $\mathbf{Q}_{\mathbf{q}(\mathbf{N})\mathbf{q}(\mathbf{N})}$ using the quaternion parametrization of the rotation matrix and the covariance propagation law.

3.5. Solution Fixing

The MC-LAMBDA algorithm outputs a set of integer ambiguities $\tilde{\mathbf{N}}$, solution of (10), and the corresponding conditional solution $\mathbf{q}(\tilde{\mathbf{N}})$. At this point of development, no validation is done regarding $\mathbf{q}(\tilde{\mathbf{N}})$. Therefore, before fixing a set of ambiguities, there is a time period where the sets output by the MC-LAMBDA are collected and stored. Afterwards, the set that occurred most often (the most ‘‘popular’’) is chosen.

The fixing is done using a second EKF update step, where $\tilde{\mathbf{N}}$ and $\mathbf{q}(\tilde{\mathbf{N}})$ are fed as pseudo-measurements. The expressions used during this step are written as

$$\begin{aligned} \mathbf{K}'_k &= \mathbf{H}'^\top (\mathbf{H}'\mathbf{P}_{k|k}\mathbf{H}'^\top + \mathbf{R}')^{-1} \\ \hat{\mathbf{x}}'_{k|k} &= \hat{\mathbf{x}}_{k|k} + \mathbf{K}'_k (\mathbf{z}'_k - \mathbf{H}'\hat{\mathbf{x}}_{k|k}) \\ \mathbf{P}'_{k|k} &= (\mathbf{I} - \mathbf{K}'_k\mathbf{H}')\mathbf{P}_{k|k}, \end{aligned} \quad (44)$$

where the residual $\mathbf{z}'_k - \mathbf{H}'\hat{\mathbf{x}}_{k|k}$ is computed as

$$\begin{aligned} \mathbf{z}'_k - \mathbf{H}'\hat{\mathbf{x}}_{k|k} &= \\ &= \begin{bmatrix} \mathbf{q}(\tilde{\mathbf{N}}) \\ \tilde{\mathbf{N}} \end{bmatrix} - \begin{bmatrix} \mathbf{I}_4 & \mathbf{0} & \mathbf{0} \\ \mathbf{0} & \mathbf{0} & \mathbf{I}_{mn} \end{bmatrix} \begin{bmatrix} \hat{\mathbf{q}}_{k|k} \\ \hat{\mathbf{b}}_{k|k} \\ \hat{\mathbf{n}}_{k|k} \end{bmatrix}. \end{aligned} \quad (45)$$

Matrix \mathbf{R}' is tuned manually so as to obtain the best compromise between improving the accuracy of the float solution, while allowing the next step of the EKF to change the state estimates, if needed, which becomes harder as the entries of \mathbf{R}' are lower.

As described, this 2nd update step builds on the EKF float solution $\hat{\mathbf{x}}_{k|k}$. The fixed solution at time t_k , $\hat{\mathbf{x}}'_{k|k}$, is then used in the propagation step of the next time step t_{k+1} , closing the loop, and the process is repeated.

4. Simulation Results

A simple simulation environment was developed, allowing evaluation of the proposed solution, since the true attitude and integer ambiguities are known *a priori*. This environment generates code and carrier phase

Baseline length [m]	1			5			10		
Code noise $\sigma_{P,i}^k$ [cm]	50	40	30	50	40	30	50	40	30
# Satellites									
5	83.96	94.75	97.30	96.85	97.23	96.81	95.41	98.37	98.29
6	93.08	98.92	98.56	98.31	98.15	97.97	98.40	97.87	99.06
7	95.05	97.34	98.77	98.18	98.97	98.55	98.42	98.53	97.67

Table 1: Integer Ambiguity Determination success rates of the developed framework under different scenarios.

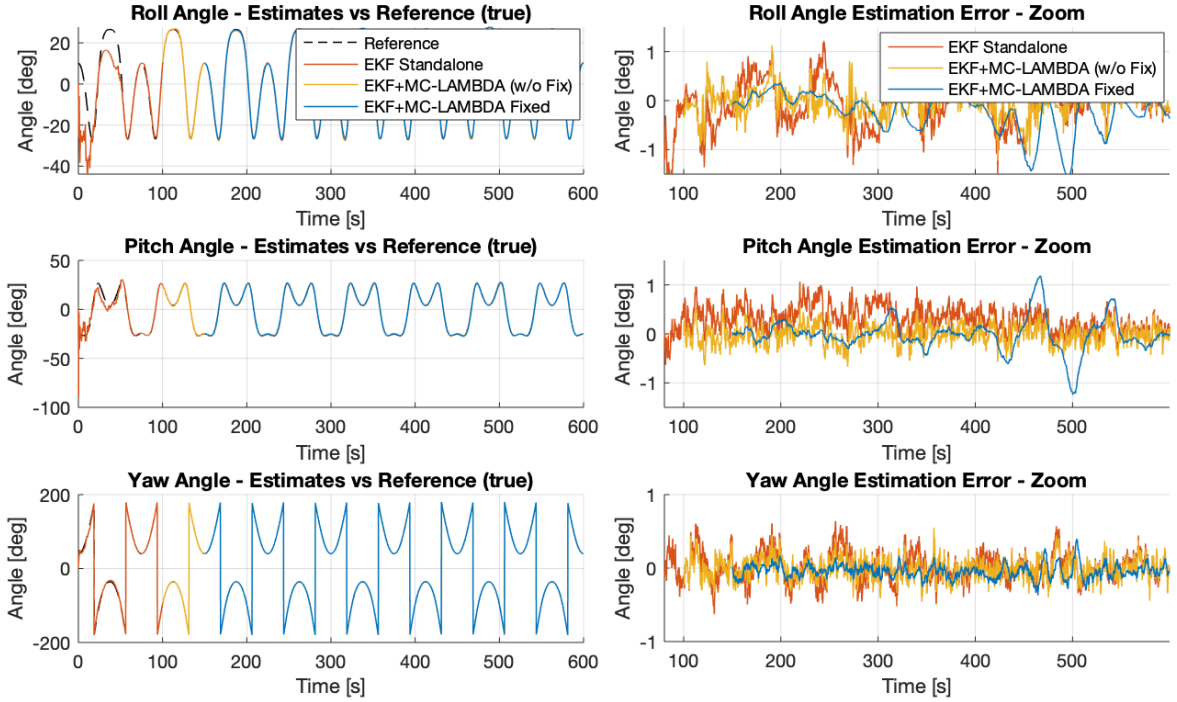


Figure 1: Dynamic trial, single baseline attitude estimates, including intermediate solutions.

measurements, as well as gyroscope measurements, according to models (2) and (12). The GNSS measurements errors are assumed white noise processes, whose variance is given by the stochastic model based on satellite elevation angle (46). The code and carrier phase variances $(\sigma_{P,i}^k)^2$ and $(\sigma_{\Psi,i}^k)^2$ are the diagonal elements of \mathbf{Q}_P and \mathbf{Q}_Ψ in (5).

$$\begin{cases} (\sigma_{P,i}^k)^2 = 100^2 \left(c_1^2 + \left(\frac{c_2}{\sin \text{el}_k} \right)^2 \right) \\ (\sigma_{\Psi,i}^k)^2 = c_1^2 + \left(\frac{c_2}{\sin \text{el}_k} \right)^2 \end{cases} \quad (46)$$

Note that navigation data collected experimentally is used to compute the satellite positions at a given epoch.

In the following, simulated data is used to evaluate the performance of integer ambiguity determination, under the proposed framework. Then, attitude estimation results corresponding to a dynamic trial are presented.

4.1. Integer Ambiguity Determination Success Rate

The MC-LAMBDA method is evaluated by computing success rates, which are the percentage of epochs in which the set of determined ambiguities are correct. The success rates in different scenarios are obtained by performing Monte Carlo simulations. In all scenarios, a single baseline $\mathbf{l}_{i1} = \|\mathbf{l}_{ik}\| [1, 0, 0]^T$ is simulated and the body is static. The length $\|\mathbf{l}_{ik}\|$, the simulated code measurements noise and number of GPS satellites in view are varied in each scenario, as shown in Table 1.

There is a clear increase in the success rates of the ambiguity determination as the measurements noise decreases or the number of tracked satellites is higher, which can be seen in the simulation results corresponding to a unitary baseline length. It is natural that having less noisy observations leads to a more accurate float solution, which is the starting point of the search process done in the MC-LAMBDA algorithm, increasing its success rate. Note that a code noise of 50 cm is quite high when compared to a baseline length of 1 m,

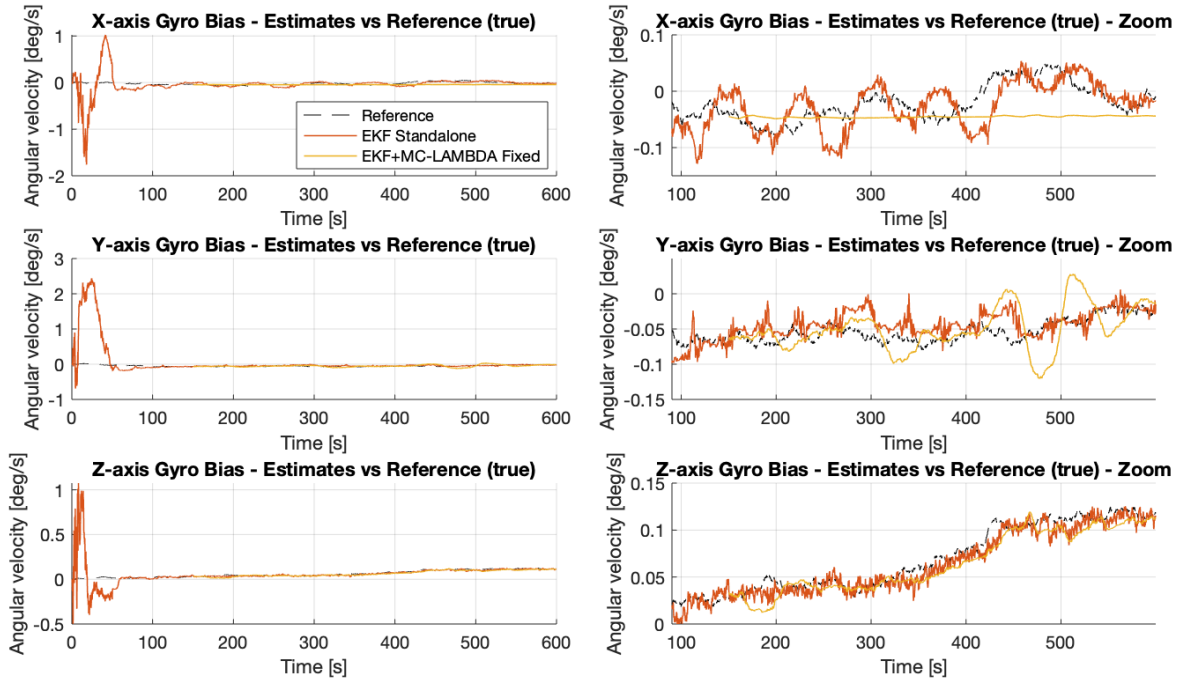


Figure 2: Dynamic trial, single baseline EKF without fixing and fixed solutions' bias estimates.

and even in this case, a high success rate of 83.96% is achieved.

As more satellites are available, more information is fed to the filter, improving the attitude estimates along with the accuracy of the integer ambiguity candidates. As for the baseline length, shorter baselines hinder correct integer ambiguity determination, since the observation model used in the EKF is highly nonlinear for very short baselines. As seen in Table 1, the overall success rate when simulating a baseline of 5 m is higher, compared to 1 m.

Given these results, it is very likely that the integer ambiguity set chosen for the fixing is the correct one, since it only needs to occur at least 50% of the time during the ambiguity storing period.

4.2. Single Baseline Dynamic Trial

In this Section, the attitude estimation results of a simulated dynamic trial are presented. As before, a single baseline $\mathbf{l}_{i1} = [1.3, 0, 0]^T$ [m] is simulated. Therefore, the results provide experimental validation of the observability properties studied before. The simulated angular kinematics of the body are presented in Figure 3.

The initial attitude of the body, in terms of Euler angles, is $(\varphi, \theta, \psi) = (10, -25, 40)$ [deg], where φ, θ, ψ are the roll, pitch and yaw angles. The initial estimate of the EKF is set at $(\varphi_0, \theta_0, \psi_0) = (0, 0, 0)$ [deg]. Then, the fixed solution as well as intermediate solution's attitude estimates are shown in Figure 1. The *EKF Standalone* solution is the EKF output without determining the integer ambiguities. Then, *EKF+MC-*

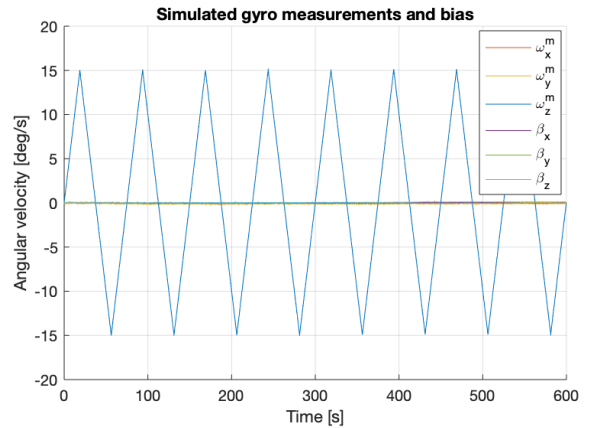


Figure 3: Simulated angular velocity measurements.

LAMBDA (w/o Fix) is the MC-LAMBDA conditional solution in time, without fixing the solution. Finally, *EKF+MC-LAMBDA Fixed* denotes the fixed solution. It is seen from Figure 1 that the full attitude is estimated using a single baseline, which is possible due to dynamic motion of the body and using a kinematics model in the EKF. The fixed solution is actually the less precise, since it reacts more slowly to the quick attitude variation. Even so, the standard deviation of the fixed solution error for the roll, pitch and yaw is 0.40° , 0.34° and 0.10° , respectively.

The float and fixed bias estimates are represented in Figure 2. The Y and Z-axis fixed solution correctly estimates the bias, while the X-axis estimate does not follow the reference. The fixing process lowers the co-



Figure 4: Trajectory and key points describing the experimental dynamic trial.

variance matrix entries of the filter, since it consists of a 2nd Update Step. As such, the filter becomes less sensitive to the angular velocity measurements.

Overall, it is clearly seen that in a dynamic scenario where the body has non-null angular acceleration around the Z-axis, it is possible to estimate the full attitude and gyro bias using a single baseline.

5. Experimental Results

Apart from using simulated data, the proposed algorithm was also validated experimentally. Due to hardware purchase restrictions, owing to the Covid-19 pandemic, only two antennas are available, and a smartphone's IMU sensor is used to measure the angular velocity. The setup used during the dynamic trial is shown in Figure 5. Two GPS antennas, the AT575-75 by AeroAntenna Technology and the 53G15A by Antcom Corporation, are used, attached to Reach Module GNSS receivers. The baseline length is 1.95 m.



Figure 5: Experimental setup used in the dynamic trial.

In the following, the dynamic trial performed using this setup, along with the attitude estimation results obtained by processing the collected data, are presented.

5.1. Dynamic Trial

A representation of the trajectory followed by the platform on which the antennas are mounted is given in Figure 4. Since a vehicle is used, the roll and pitch angles are constricted by the terrain. In order to further excite the relative orientation of the antennas, slight nudges are manually given at certain points along the trajectory, represented with a star in the figure. The start and end points are denoted by the red and yellow squares, respectively.

The fixed solution corresponding to the attitude estimate of the body along this trajectory is shown in Figure (6). The vertical dashed lines coincide with the periods in which the baseline is manually excited, or the stars in Figure (4). After around $t = 100$ s, the filter's estimate starts converging to the correct attitude, as the yaw angle estimate approaches -60° . After convergence, each turn and roundabout done during the trajectory of the vehicle is clearly seen in the 90° and 180° variations of the estimated heading. Concerning the pitch estimate, it is close to 0° , as expected, since the terrain's inclination is very low. Comparing the results with the trajectory, the pitch and yaw are clearly correctly estimated. In regards to the roll angle, which coincides with the non-observable axis if the body were static, it is seen that the angular motion keeps the roll angle estimate close to 0° . As expected, after around $t = 530$ s, when the vehicle stops, the roll angle starts to diverge. As such, the observability properties studied analytically are confirmed experimentally.

6. Conclusions

Throughout this work, a novel solution for GNSS-based attitude estimation was detailed, where an EKF fed by angular velocity and carrier phase measurements is integrated with the MC-LAMDBA method.

A preliminary study of the observability of the filter was done by analyzing the observability properties of

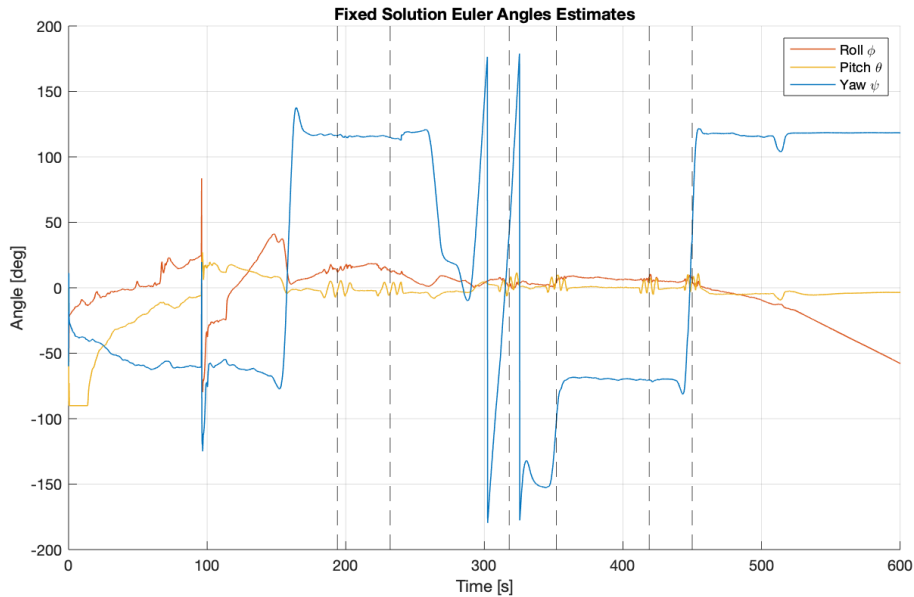


Figure 6: Fixed solutions' estimated Euler angles during the dynamic experiment.

a linearized system model. It was concluded that in a static, single baseline scenario, the full attitude and 3-axes gyro bias are not observable. In the multiple baseline case, under the static assumption, the state is found to be observable. Further validations are done experimentally.

The developed framework implies IAD success rates of at least 83.96%, even in the most demanding case, where the code noise is comparable to the baseline length. The integration of the gyroscope measurements in the kinematics model underlying the EKF allowed a precise estimation of the attitude. Sub degree precisions were achieved in the demanding single baseline scenario, using single-frequency receivers.

In the future, a complete analysis of the observability properties of the system in a dynamic scenario must be done. Techniques suitable for analyzing nonlinear systems can be employed. Further experimental validation, using more GNSS antennas and receivers, as well as a better gyroscope, would allow a finer evaluation of this solution. Finally, validation of the MC-LAMBDA integer ambiguities solution would enhance the framework, as the time period where sets of ambiguities are stored, prior to fixing, would no longer be required.

References

- [1] P. Axelrad and L. M. Ward. Spacecraft attitude estimation using the global positioning system - methodology and results for RADCAL. *Journal of Guidance, Control, and Dynamics*, 19(6):1201–1209, 1996.
- [2] A. Gelb and T. A. S. Corporation. *Applied Optimal Estimation*. The MIT Press, 1974.
- [3] G. Giorgi and P. Teunissen. *GNSS Carrier Phase-Based Attitude Determination*. February 2012.
- [4] R. Hermann and A. Krener. Nonlinear controllability and observability. *IEEE Transactions on Automatic Control*, 22(5):728–740, 1977.
- [5] C. Park and P. Teunissen. A baseline constrained LAMBDA method for an integer ambiguity resolution of GNSS attitude determination systems. *Journal of Institute of Control, Robotics and Systems*, 14:587–594, 06 2008.
- [6] P. Schönemann. A generalized solution of the orthogonal procrustes problem. *Psychometrika*, 31(1):1–10, 1966.
- [7] T. Suzuki, Y. Takahashi, and Y. Amano. Precise UAV position and attitude estimation by multiple GNSS receivers for 3D mapping. pages 1455–1464, 11 2016.
- [8] P. Teunissen. The least-squares ambiguity decorrelation adjustment: A method for fast GPS integer ambiguity estimation. *Journal of Geodesy*, 70:65–82, 11 1995.
- [9] P. Teunissen. A general multivariate formulation of the multi-antenna GNSS attitude determination problem. *Artificial Satellites*, 42:97–111, 01 2007.
- [10] S. A. Whitmore and L. Hughes. United States Patent - Closed-form Integrator for the Quaternion (Euler Angle) Kinematics Equations, 2000.